Enhanced robustness and dimensional crossover of superradiance in cuboidal nanocrystal superlattices

Sushrut Ghonge[1,*] David Engel[1] Francesco Mattiotti[2] G. Luca Celardo[3] Masaru Kuno[1,4] and Boldizsár Jankó[1,†]

[1]*Department of Physics and Astronomy, University of Notre Dame, Notre Dame, Indiana 46556, USA*
[2]*University of Strasbourg and CNRS, CESQ and ISIS (UMR 7006), aQCess, 67000 Strasbourg, France*
[3]*Department of Physics and Astronomy, University of Florence, INFN, Florence Section, and CSDC, Via Sansone 1, 50019 Sesto Fiorentino, Firenze, Italy*
[4]*Department of Chemistry and Biochemistry, University of Notre Dame, Notre Dame, Indiana 46556, USA*

(Received 21 September 2022; accepted 28 February 2023; published 27 April 2023)

Cooperative emission of coherent radiation from multiple emitters (known as superradiance) has been predicted and observed in various physical systems, most recently in $CsPbBr_3$ nanocrystal superlattices. Superradiant emission is coherent and occurs on timescales faster than the emission from isolated nanocrystals. Theory predicts cooperative emission being faster by a factor of up to the number of nanocrystals (N). However, superradiance is strongly suppressed due to the presence of energetic disorder, stemming from nanocrystal size variations and thermal decoherence. Here, we analyze superradiance from superlattices of different dimensionalities (one-, two-, and three-dimensional) with variable nanocrystal aspect ratios. We predict as much as a 15-fold enhancement in robustness against realistic values of energetic disorder in three-dimensional (3D) superlattices composed of cuboid-shaped, as opposed to cube-shaped, nanocrystals. Superradiance from small ($N \lesssim 10^3$) two-dimensional (2D) superlattices is up to ten times more robust to static disorder and up to twice as robust to thermal decoherence than 3D superlattices with the same N. As the number of N increases, a crossover in the robustness of superradiance occurs from 2D to 3D superlattices. For large N ($>10^3$), the robustness in 3D superlattices increases with N, showing cooperative robustness to disorder. This opens the possibility of observing superradiance even at room temperature in large 3D superlattices, if nanocrystal size fluctuations can be kept small.

DOI: 10.1103/PhysRevResearch.5.023068

I. INTRODUCTION

In 1954, Dicke [1] predicted a phenomenon he termed superradiance (SR), which involves a collection of identical light emitters spontaneously emitting intense coherent radiation. Since then, superradiance has been observed in various physical systems such as molecular aggregates [2,3], cold atoms [4], diamond nanocrystals [5], semiconductor quantum dot ensembles [6,7], and more recently, in both nanocrystal (NC) superlattices [8–10] and hybrid perovskite thin films [11]. SR can be used to develop ultra-narrow-linewidth lasers for quantum metrology [12], efficient light-harvesting and photon detecting devices [13], and is key to recently proposed sunlight-pumped lasers [14].

Typically, the probability density that a single excited particle emits a photon is exponentially distributed and is characterized by a lifetime τ. If there are N entangled emitters, all in the excited state, SR theory predicts cooperative emission with $\sim N^2$ times higher peak intensity than that of a single emitter (in contrast to $\sim N$ for unentangled emitters). If the incident radiation is so weak that only one excitation is present, single-excitation superradiance [15] can result. In this case, if the excitation is coherently shared by N emitters, its lifetime decreases by a factor of N and, in turn, causes the emission intensity to scale by the same factor.

Experimentally, superfluorescence (a type of superradiance where emitting dipoles are spontaneously entangled) has recently been observed in three-dimensional (3D) superlattices of $10^6 - 10^8$ cube-shaped $CsPbBr_3$ NCs [8]. At low fluence, the observed radiative decay rate is only a factor of three faster than that of individual nanocrystals. This is several orders of magnitude smaller than what is predicted from a linear N scaling. We have recently shown that this deviation can be rationalized [16].

We use the radiative Hamiltonian approach to model SR from NC superlattices, which is valid for all systems sizes in the point-dipole approximation. This is in contrast to static dipole-dipole coupling, used by, for example, Blach *et al.* [17], which is only valid for distances smaller than the emission wavelength. The radiative Hamiltonian was first used to study lattices of atomic dipoles [18–20] and then successfully applied to study superradiance from perovskite NC superlattices [16] by some of the authors of the present paper. Sierra *et al.*

*sghonge@nd.edu
†bjanko@nd.edu

[21] also use a similar Hamiltonian to study the effect of dimensionality on the critical distance needed to yield superradiance in arrays of atoms that have a single excited state, whereas we model isotropic emission from NCs by considering three excited states along x, y, and z directions.

Through detailed modeling, we find that both energetic disorder, stemming from NC size and band-gap variations, as well as the collective effects of thermal decoherence (i.e., thermal noise due to a finite temperature) suppress SR rate enhancements. Thus while superradiant enhancements of up to $O(10^3)$ are possible with a few thousand coupled NCs in a superlattice, thermal decoherence and static disorder bring this enhancement factor down to $O(1)$.

Having established the origins of a smaller than expected superradiant enhancement, we discuss approaches to overcoming this suppression. SR occurs when nanocrystals couple with each other through interactions between their transition dipoles. Dipole-dipole interaction strengths are inversely proportional to the cube of their separation. Bringing dipoles closer therefore increases the coupling and should make superradiance more robust to disorder. The interaction also depends on the relative orientations of the dipoles, as well as the angles between them and the mutual vector joining them. If NCs are all arranged in a line (one dimension, 1D) or a plane (two dimensions, 2D), all vectors joining dipoles lie on the same line or in the same plane, respectively. This changes the structure of dipolar couplings and affects how systems respond to static and thermal disorder.

In this study we establish how changing superlattice dimensionality affects superradiance and its robustness to static and thermal disorder. We also investigate the effect changing component NC aspect ratios has on SR and its robustness. This is done by simulating SR from cuboidal NC superlattices. Our results show an interplay between superlattice dimensionality and NC shape on SR enhancement. We show that superlattices of cuboidal NCs are more superradiant and more robust to static and thermal disorder for any number of NCs. Moreover, SR from 2D superlattices can be more robust to disorder if they are composed of a small number of NCs ($N < 10^3$). On the other hand, for large superlattices, robustness to disorder increases with superradiant decay rate. This effect has been predicted previously and is known as "cooperative robustness" [22–24]. Here we demonstrate cooperative robustness in a realistic model of perovskite superlattices. Since 3D superlattices show larger increases of the superradiant decay rate with system size, they possess cooperative robustness that can yield superradiance even in the presence of disorder, having energies comparable to room-temperature thermal energy.

II. THEORETICAL MODEL AND NUMERICAL METHODS

A superlattice is defined here as a lattice consisting of N_x, N_y, and N_z NCs self-assembled along x, y, and z directions, respectively. Corresponding NC center-to-center distances are a_x, a_y, and a_z, which are sums of NC edge lengths and interparticle spacings along a given direction. The total number of NCs (N) in a superlattice is $N = N_x \times N_y \times N_z$.

When $N_x = N_y = N_z > 1$, the arrangement is said to be a regular 3D superlattice. If the number of NCs along any one edge (say N_z) is equal to 1, and $N_x = N_y > 1$, the arrangement is a regular 2D superlattice. In a 1D superlattice, NCs are arranged only along one direction (say, $N_x = N_y = 1 < N_z$). Figure 1 illustrates superlattices of different dimensionalities.

We define superlattice aspect ratio, ρ, as the ratio of center-to-center distance along shorter and longer superlattice axes. In 3D we assume that center-to-center distances along x and y axes (e.g., a_x and a_y) are equal so that $\rho \equiv a_z/a_x$. In 2D, there are only two axes (e.g., x and y). Consequently, $\rho = a_x/a_y$. In 1D, aspect ratio is not defined because there is only one axis. Figure 1 shows the various ways in which one can arrange cuboidal NCs into superlattices with different ρ values.

SR from NC superlattices is modeled via lattices of interacting transition dipoles. Such dipole lattices have previously been studied theoretically and reveal the emergence of cooperative behavior when lattices are free of disorder [18–20]. In these models each lattice site has a point dipole that can be oriented in one of three directions (x, y, or z). Point dipoles interact via their mutual radiation field. In this way, SR from cold atomic clouds has been predicted and modeled [25–27].

Modeling is done in the so-called "single-excitation superradiance" regime to capture behavior induced by low excitation intensities employed in actual measurements [28,29]. In this limit there is only one excited NC in the superlattice. This simplification reveals relevant SR trends because the involved Hilbert space scales as N, in contrast to the 2^N scaling in the high-fluence limit. The approach has previously allowed us to numerically study large superlattices of $\sim 10^4$ interacting dipoles [16].

NCs with edge lengths of $l = 9$–29 nm are studied [9,30–32]. This corresponds to center-to-center distances of 10–30 nm, assuming an interparticle spacing of 1 nm. Such NCs lie in the intermediate-to-weak confinement regime given a $CsPbBr_3$ Bohr exciton radius (a_B) of 3.5 nm [30,33]. For NC dimensions above a_B, band gaps do not vary significantly [33], allowing an assumption that transition dipole moments are size independent [16]. The spacing between NCs is due to a coating of organic ligands, specifically oleic acid and oleylamine [8,34,35]. The optical dielectric constants of $CsPbBr_3$ [33], oleic acid [36], and oleylamine [37] are 4.8, 3.1, and 2.13, respectively. The exciton structure and coupling can be affected by this dielectric mismatch when the size of the NCs is smaller that the exciton Bohr radius [38], thus being another reason for us to only consider larger NCs.

We use following non-Hermitian Hamiltonian [16] to model the NC superlattice,

$$\hat{H} = \hbar\left(\omega_0 - i\frac{\gamma_r}{2}\right)\sum_{\alpha}\sum_{n=1}^{N}|n,\alpha\rangle\langle n,\alpha| + \sum_{\alpha,\beta}\sum_{\substack{m,n=1\\ m\neq n}}^{N} J_{mn}^{\alpha\beta}|m,\alpha\rangle\langle n,\beta|, \quad (1)$$

where $\hbar\omega_0 (\equiv E_0)$ is the NC band gap, γ_r is the single NC radiative decay rate, and $\alpha, \beta = x, y, z$ are transition dipole directions. $J_{mn}^{\alpha\beta}$ terms, which indicate the coupling between

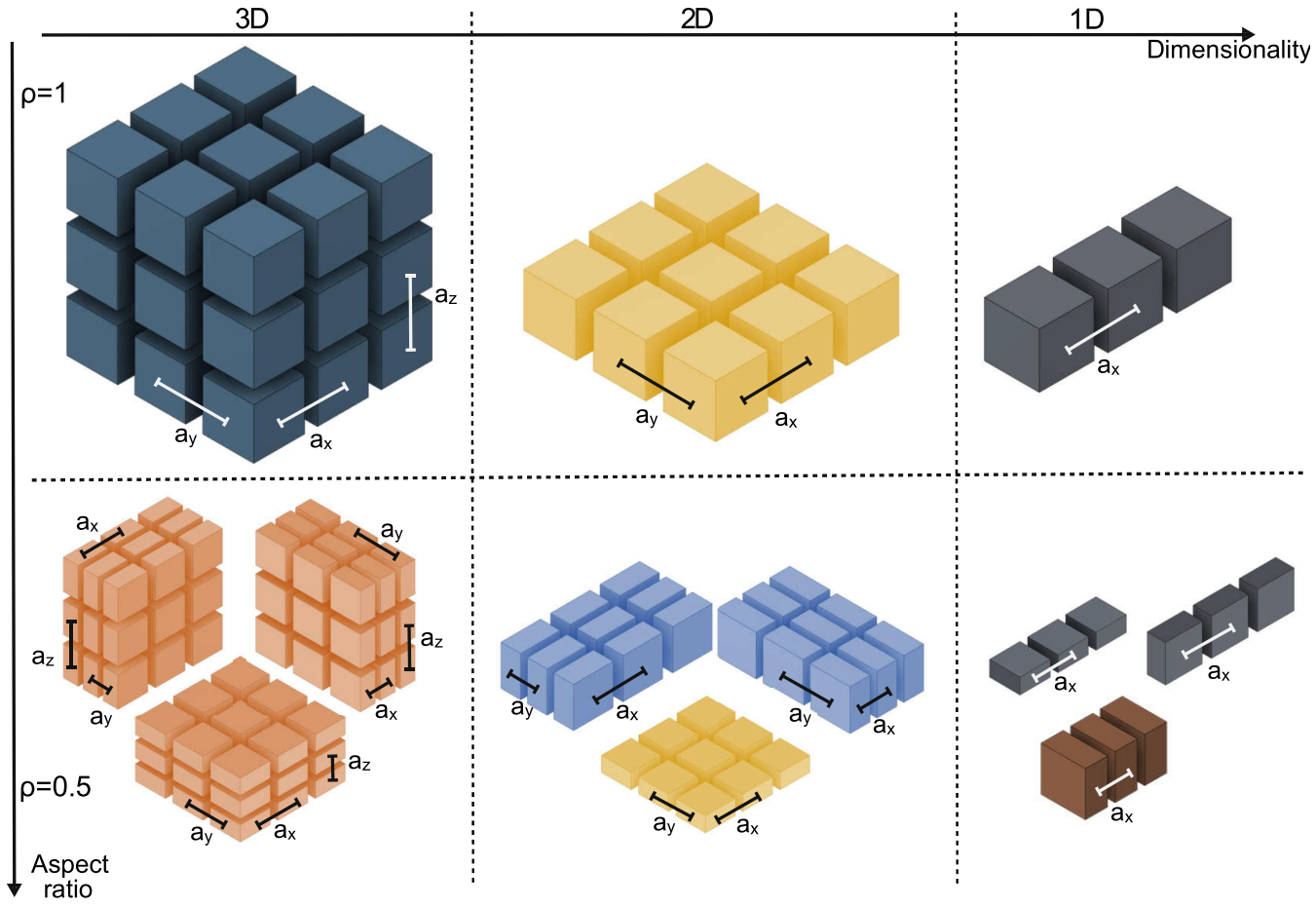

FIG. 1. Schematic figures showing superlattices with different dimensionalities and center-to-center distances. The top row shows superlattices of cubic NCs, while the bottom row shows superlattices of cuboidal NCs. The key parameters in our model, the center-to-center distances along different axes, are labeled on all figures. In 3D, the three different ways to arrange cuboidal NCs into a superlattice are all equivalent (orange figures). In 2D there is one way to arrange cuboidal NCs (yellow) that does not change the center-to-center distances and two equivalent ways (blue) that do. In 1D there is only one way (brown figure) to arrange cuboidal NCs that modifies the center-to-center distance.

NCs, are given by

$$\mathrm{Re}J_{mn}^{\alpha\beta} = \frac{\hbar\gamma_r}{2}\left[y_0(kr_{mn})\hat{e}_\alpha\cdot\hat{e}_\beta - \frac{1}{2}y_2(kr_{mn})g_{mn}^{\alpha\beta}\right], \quad (2)$$

$$\mathrm{Im}J_{mn}^{\alpha\beta} = -\frac{\hbar\gamma_r}{2}\left[j_0(kr_{mn})\hat{e}_\alpha\cdot\hat{e}_\beta - \frac{1}{2}j_2(kr_{mn})g_{mn}^{\alpha\beta}\right]. \quad (3)$$

Here, $g_{mn}^{\alpha\beta}$ denotes the geometric factor $[\hat{e}_\alpha\cdot\hat{e}_\beta - 3(\hat{e}_\alpha\cdot\hat{r}_{mn})(\hat{r}_{mn}\cdot\hat{e}_\beta)]$, and y_ν and j_ν are spherical Bessel functions of order ν. $\vec{r}_{mn}$ is the vector joining the centers of the mth and nth NCs (r_{mn} and $\hat{r}_{mn}$ are the magnitude of $\vec{r}_{mn}$ and the unit vector along $\vec{r}_{mn}$, respectively), and $k = \frac{2\pi}{\lambda}$ is the radiation wave number inside the material. The vectors $\vec{r}_{mn}$ depend on the superlattice parameters a_x, a_y, and a_z, that we defined above. In our model, when we change the NC sizes and aspect ratios, the corresponding center-to-center distances $\vec{r}_{mn}$ will also change. $CsPbBr_3$ parameters of $E_0 = 2.38$ eV and $\lambda = 237$ nm are used, corresponding to a vacuum wavelength of 520 nm [8] for a refractive index of 2.2 [33]. Note that the model is general and applicable to any NC superlattice provided appropriate material parameters.

Equation (2) is a generalized dipole-dipole coupling term. For small distances ($kr_{mn} \ll 1$), such as when we consider the nearest-neighbor coupling, it is the usual dipole-dipole interaction that is proportional to $1/r_{mn}^3$. The imaginary term, Eq. (3), arises due to the field-mediated interaction between dipoles. We define the nearest-neighbor coupling ($\mathcal{J}$) as the maximum coupling between transition dipoles of neighboring NCs, $\mathcal{J} = \max_{\alpha,\beta}\{|J_{m,m+1}^{\alpha\beta}|\}$. The real part of the nearest-neighbor coupling is much greater than the imaginary part. For example, when the center-to-center distance (say, a_x) is 10 nm, $\mathcal{J}$ is about 0.14 meV. When the center-to-center distance is 5 nm, $\mathcal{J}$ becomes 1.1 meV.

Diagonalizing $\hat{H}$ yields complex eigenvalues (denoted by Λ), whose imaginary parts reflect NC decay rates. Real parts represent the corresponding energy of emitted radiation. States that decay faster or slower than a single NC are called *superradiant* or *subradiant*, respectively. The maximum SR rate, denoted by Γ_{SR}, is defined as $\Gamma_{SR} \equiv \max[-\mathrm{Im}\Lambda]/(\hbar/2)$. The corresponding energy equivalent, $\hbar\Gamma_{SR}$, is called the superradiant decay width. Γ_{SR} is normalized by the emission rate of an individual, noninteracting NC to obtain a

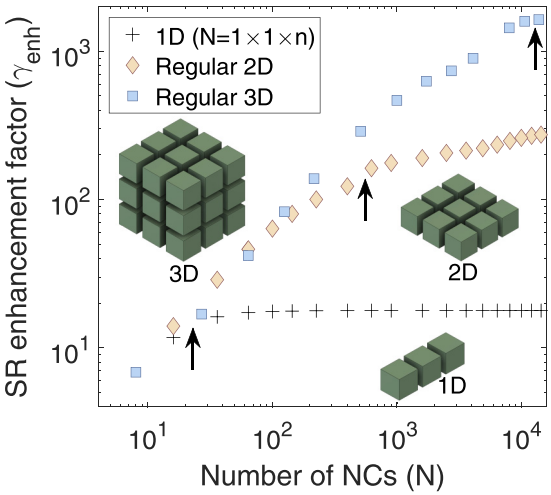

FIG. 2. Comparison of the maximum possible SR enhancement from different superlattice dimensionalities composed of cube-shaped NCs with a center-to-center distance of 10 nm (i.e., $a_x = a_y = a_z = 10$ nm). Insets show illustrations of NC superlattices with 1D, 2D, and 3D dimensionalities. The arrows indicate when the length of the superlattice becomes equal to the wavelength of incident radiation ($N = 23$ in 1D, $N = 561$ in 2D, and $N = 1.33 \times 10^4$ in 3D).

dimensionless SR enhancement factor $\gamma_{enh} = \frac{\Gamma_{SR}}{\gamma_r}$. We also define the spectral width as the range of the real parts of the eigenvalues, $\Delta\mathcal{E} = \max[\mathrm{Re}\{\Lambda\}] - \min[\mathrm{Re}\{\Lambda\}]$.

SR energy shifts are obtained from the real parts of the eigenvalues using $\Delta E = \mathrm{Re}\Lambda - E_0$. SR redshifts of 0.3 meV are predicted, which do not reproduce the much larger redshifts observed in practice by Rainò *et al.*, and Baranov *et al.* [35]. We have therefore previously rationalized larger than expected SR redshifts as due to SR from small, interacting NC subensembles within superlattices [16].

III. RESULTS AND DISCUSSION

A. Superradiance in the absence of disorder

1. *Influence of superlattice dimensionality*

Figure 2 shows how superlattice dimensionality impacts γ_{enh} for assemblies consisting of cube-shaped $CsPbBr_3$ NCs with a center-to-center distance of 10 nm. Superradiance from three superlattice dimensionalities is compared, where the total number of NCs ranges from 4 to 1.5×10^4. The figure shows that for large N, the 3D superlattice is the most superradiant in absolute terms. This is followed by 2D and 1D superlattices in this order.

Our model correctly captures a deviation from the linear increase of γ_{enh} [16] as the system size becomes comparable with λ (the wavelength of radiation inside the material), see arrows in Fig. 2. For the 1D superlattice, saturation occurs when $N \times a$ (the length of the superlattice) results in a physical distance of order λ. This is in agreement with an analogous result for atomic lattices [21]. At small N where the entire superlattice is smaller than the wavelength of light, γ_{enh} is roughly equal for all three superlattice dimensionalities and increases linearly with N.

One can also visualize the wave function corresponding to different eigenstates of the Hamiltonian [Eq. (1)] for 2D superlattices. Supplementary Material (SM) [47] Figs. S1 and S2 show the real and imaginary parts of the wave function corresponding to the most superradiant and a typical strongly subradiant state. The wave function corresponding to the most superradiant state has the fewest possible nodes for the size of the superlattice, while that of a subradiant state oscillates with a much smaller wavelength.

2. *Dependence on NC aspect ratio*

We now study the dependence of γ_{enh} on NC aspect ratio for the 3D and 2D superlattices first considered in Fig. 2. It is known that colloidal syntheses produce NCs with variable aspect ratios. Classic examples include CdSe nanorods [39], nanoplatelets [40,41], and nanowires [42–44], and more recently, $CsPbBr_3$ platelets [9,31]. It has also been possible to self-assemble such cuboidlike NCs into superlattices [9,32].

In our model, $\hat{H}$ [Eq. (1)] depends only on the NC center-to-center distance ($\vec{r}_{mn}$). The aspect ratio (ρ) implicitly takes into account NC shape and interparticle spacings due to the presence of organic ligands. In the results that follow, the number of NCs along each edge of a superlattice remains constant. Therefore the overall aspect ratio of the superlattice is equal to the ratio of NC center-to-center distances. In all cases, NC dimensions are greater than a_B so that strong confinement effects can be ignored. For the same reason, we assume that NC transition dipoles do not change significantly.

Figure 3(a) now reveals that as ρ decreases from $\rho =$ 1–0.4, γ_{enh} increases. The reason for this increase in γ_{enh} is the decrease in NC center-to-center distance along one direction, which increases the number of NCs (and hence emitters) per unit volume. Conversely, increasing center-to-center distances reduces NC densities and suppresses γ_{enh}. Figure 3(b) shows that γ_{enh} increases are even more significant when low-aspect-ratio NCs are arranged into 2D superlattices. See Supplementary Material (SM) Fig. S3 for the dependence of γ_{enh} on ρ in 1D, which is equivalent to changing the NC center-to-center distance along the superlattice direction.

Even though we predict a monotonic increase in superradiant enhancement as NC aspect ratio decreases, we have avoided more extreme aspect ratios where we expect strong confinement in one (nanosheets) or two (nanowires) dimensions [45,46]. In such systems the response to light of the NCs might become anisotropic.

B. Robustness to static disorder

We now investigate SR robustness to static disorder for superlattices with different dimensionalities. In practice, a finite NC size distribution exists within a superlattice. For example, in the superlattices used by Rainò *et al.* [8], the size of the NCs was 9.45 ± 0.41 nm. This size variation, in turn, introduces electronic disorder into the system due to the size dependency of NC band gaps [30]. In the intermediate-to-weak confinement regimes, this disorder is of the order of a few meV, which is much smaller than the band gap but is comparable to the coupling between NCs. In order to model this variation in band gaps, we add a random excitation energy w to our Hamiltonian matrix [Eq. (1)]. The value of

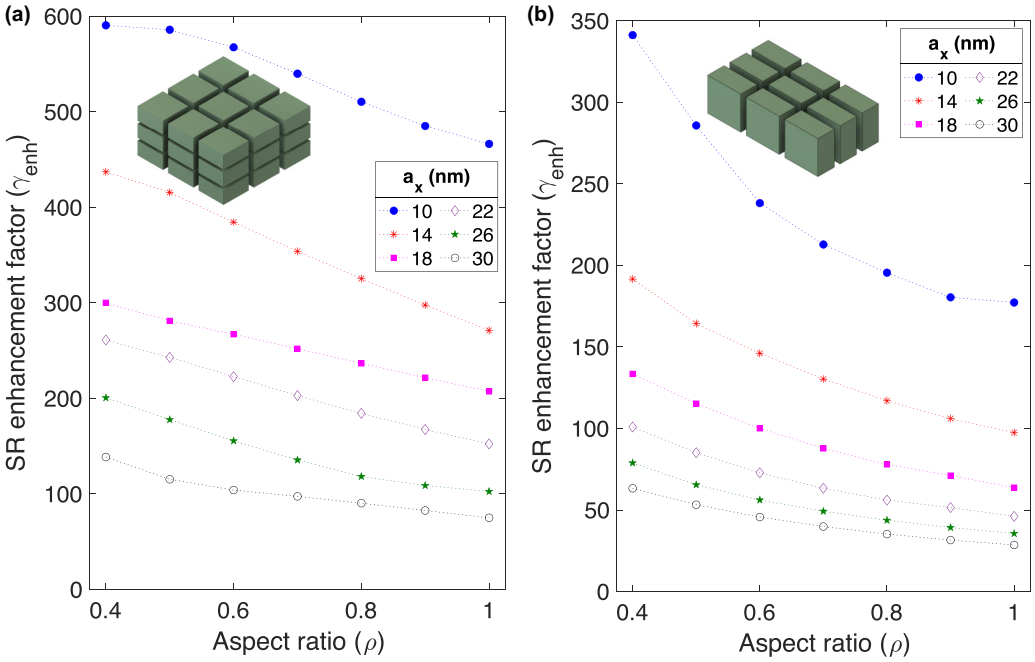

FIG. 3. Comparison of the maximum possible superradiant enhancement from NCs of different shapes, all arranged in (a) a regular 3D superlattice with 10 NCs along each side ($N = 1000$, $N_x = N_y = N_z = 10$); (b) a regular 2D superlattice with 32 NCs along each side ($N = 1024$, $N_x = N_y = 32$, $N_z = 1$), we use the perfect square that is closest to 1000. [Figure 2 shows that such a small change in N does not lead to any significant changes in the superradiance rate, so we can compare plots (a) and (b).] The center-to-center distance on the x axis of the plots refers to the two longer distances (a_x and a_y). The insets show (a) regular 3D and (b) regular 2D superlattices composed of cuboidal NCs.

w ranges from 0 to 8 meV [16]. The Hamiltonian with disorder, $H^{\alpha\beta}_{mn}(w) = H^{\alpha\beta}_{mn} + \delta_{\alpha\beta}\delta_{mn}W^{\alpha}_{m}$, where W^{α}_{m} are uniformly distributed random real numbers on the domain $[-w/2, w/2]$. For the values of N that we simulate in this paper, the superradiant enhancement becomes negligible at about 8 meV, and hence systems with even greater static disorder are not simulated.

1. Robustness in small superlattices

Figure 4(a) shows the relative robustness of 3D, 2D, and 1D cubic NC superlattices to w. For $N \sim 225$, a 2D superlattice shows a higher robustness to static disorder than a corresponding 3D superlattice of the same size. This robustness may be a consequence of the fact that superradiant states lie near the edges of the spectrum in 2D superlattices, where the density of states is low. On the other hand, 3D superlattices have fewer superradiant states and they lie close to the center of the spectrum, where density of states is higher. Therefore the superradiant states in 3D superlattices are more susceptible to mixing with other eigenstates induced by static disorder. This property is illustrated in SM [47] Fig. S4.

This increased robustness has limitations. When N is large, SR from 2D superlattices becomes sublinear and is less than that from 3D superlattices, as shown in Fig. 2. A higher robustness to static disorder is insufficient to overcome this sublinear scaling, resulting in 3D superlattices having greater superradiance, despite being less robust to static disorder (see SM [47], Fig. S5).

Next we study the sensitivity of 3D superlattice SR robustness to NC aspect ratio and static disorder. We show results for $N = 729$, because 3D superlattices are more superradiant than 2D or 1D in this regime. The results are qualitatively identical for other values of N (see SM [47], Fig. S6). Figure 4(b) shows that 3D superlattices, consisting of cuboidal NCs (e.g., $\rho = 0.5$), are as much as 15 times more robust than corresponding 3D superlattices made of cube-shaped ($\rho = 1$) NCs for realistic [16] disorder values (2 meV $< w <$ 4 meV). This is to be contrasted to the $w = 0$ case where only a $\sim$25% enhancement is seen for $\rho = 0.5$ vs $\rho = 1$ [cf. Fig. 3(a)]. This robustness to static disorder is further enhanced when cuboidal NCs are arranged into a 2D superlattice [see SM [47], Fig. S7(a)].

Smaller aspect ratio cuboidal NCs are more robust to static disorder due to the increased coupling between NCs. To confirm this, we plot γ_{enh} with respect to static disorder rescaled by the nearest-neighbor coupling ($w/\mathcal{J}$). For small N, γ_{enh} depends on the aspect ratio only through $w/\mathcal{J}$, as shown in SM [47], Fig. S6. This simple scaling does not work for large N [see Fig. S6(c)]. As we discuss in the next section, cooperative robustness plays a role when N is large.

2. Robustness in large superlattices: Cooperative robustness

We now examine how robustness to static disorder scales with number of NCs in the superlattice for a fixed geometry. Figure 4(c) shows the relative robustness of SR to static disorder for different N in 3D superlattices of cubic NCs. We see that as N increases, robustness to static disorder w [measured through $\gamma_{enh}(w)$] increases proportionally with the superradiant decay rate in the absence of disorder [$\gamma_{enh}(0)$]. This indicates the presence of cooperative robustness [22–24], which occurs when the superradiant decay width ($\hbar\Gamma_{SR}$) is

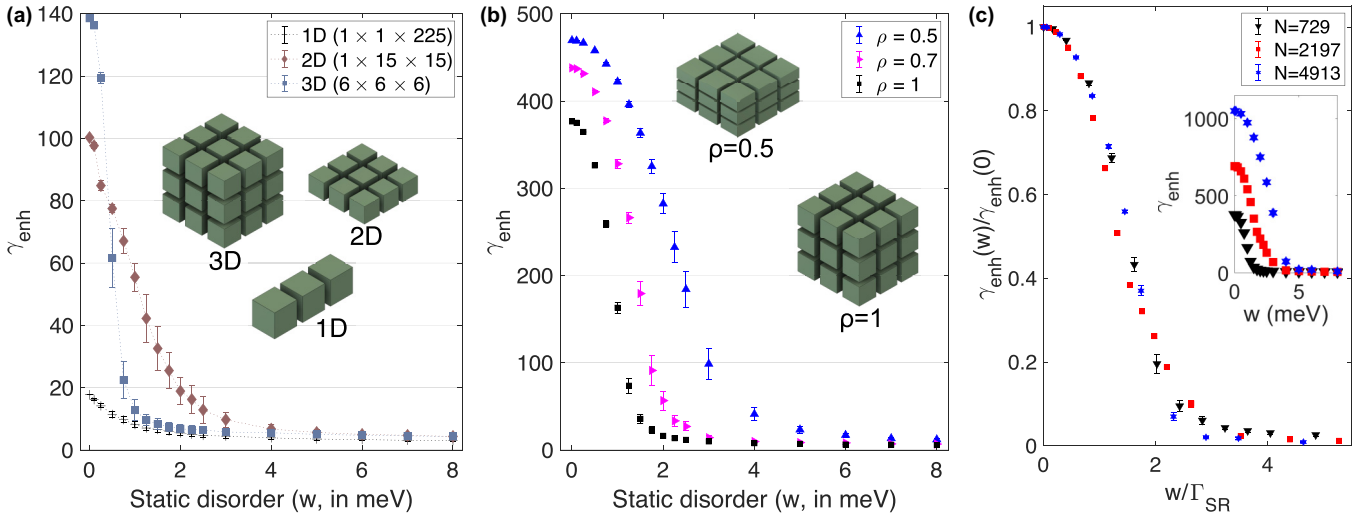

FIG. 4. Comparison of the robustness of the superradiant enhancement factor (γ_{enh}) to static disorder in superlattices of (a) different dimensionalities ($N = 216/225$, $a_x = a_y = 10$ nm), (b) different NC aspect ratios ($N = 729$, $a_x = a_y = 10$ nm), and (c) different N (3D superlattices of cubic NCs with $a_x = a_y = a_z = 10$ nm). In panel (c), the superradiant enhancement is normalized by its value in the absence of static disorder and the static disorder is normalized by the SR decay width, while the inset shows the absolute values on both axes. The error bars in all plots show the standard deviation of the eigenvalues over different disordered configurations.

much greater than the nearest-neighbor coupling ($\mathcal{J}$) [22] (see SM [47], Fig. S8). The same effect is not seen in 2D superlattices (see SM [47], Fig. S9) due to the sublinear scaling of SR with N.

The origin of this effect can be qualitatively explained as follows: A very large decay width implies a large coupling of the system with the electromagnetic field. Such strong coupling protects the system from disorder, which must become comparable in magnitude to suppress SR. In more mathematical terms, one can show that a large decay rate implies that the superradiant eigenvalue is more separated from other eigenvalues of the system in the complex plane, producing a gap along the imaginary axis. When static disorder becomes comparable to the difference between the energies of the eigenvalues of the system, superradiance is suppressed. The presence of a gap along the imaginary axis therefore protects the system with respect to disorder, similar to an energy gap along the real axis [24].

Figure 4(c) shows that in 3D superlattices, γ_{enh} is reduced to half of its disorder-free value when static disorder is about 1.5 times the superradiant decay width ($w \approx \hbar\Gamma_{SR}$). This suggests that superradiance can resist static disorder of the order of thermal energy (k_BT) at room temperature for a large 3D superlattice. The number of nanocrystals in realistic superlattices is at least 10^6, for which there can be a γ_{enh} of 10^4 in the absence of static disorder [16]. Given that the natural decay width ($\hbar\gamma_r$) of a single perovskite nanocrystal corresponds to 1.6×10^{-3} meV, this leads to a SR decay width ($\hbar\Gamma_{SR}$ of about 16 meV). Thus, for $w = 24$ meV (approximately the room-temperature thermal energy) large superradiant enhancements are possible. For example, if the average size is 10 nm, then an NC size variation of 10% (20%), that is 10 nm ± 1 nm (10 nm ± 2 nm), produces a static disorder of 25 meV (50 meV) [30].

Cuboidal superlattices produce even stronger superradiance and as a result show an even greater cooperative robustness to static disorder (see SM [47], Fig. S9). In large 3D superlattices of NCs with $\rho = 0.5$, the SR decay width $\hbar\Gamma_{SR}$ is about 24 meV, and they can show large SR enhancements for up to $w = 48$ meV, which is approximately the static disorder when the NC size variation is 10 nm ± 2 nm.

C. Robustness to thermal disorder

Given that any potential application of SR requires robustness to temperature, the robustness of SR to thermal disorder is investigated by defining a thermally averaged superradiance rate [16], denoted Γ_{TH}. This is an average superradiant decay rate, weighted by Boltzmann distributions in energy:

$$\Gamma_{TH} = -\frac{2}{\hbar}\frac{\sum_{j=1}^{3N} \mathrm{Im}\Lambda_j e^{-\mathrm{Re}\Lambda_j/k_BT}}{\sum_{j=1}^{3N} e^{-\mathrm{Re}\Lambda_j/k_BT}}. \quad (4)$$

Γ_{TH} captures the effects of a nonzero temperature on SR. Equation (4) is only valid when thermalization, which typically occurs on the picosecond timescale [30], is faster than other relaxation processes in the NC. This is usually true when the superradiant decay rate is smaller than the thermalization rate ($\gamma_{enh} < 10^3$) [16].

We define a thermal enhancement factor, similar to γ_{enh}, as $\gamma_{TH} = \Gamma_{TH}/\gamma_r$. Figure 5(a) now plots γ_{TH} for different superlattice dimensionalities. We observe that 1D and 2D superlattices are more robust to thermal decoherence than 3D superlattices for $N \simeq 216$. The qualitative trend remains the same for smaller N. However, when N becomes large (e.g., $N = 729$) 3D superlattices show the greatest superradiance (see SM [47], Fig. S10).

To understand why superradiance from 2D superlattices is more robust to thermal disorder than their 3D counterparts, we study the spectra of the corresponding Hamiltonians. The spectra of the Hamiltonians in the complex plane show the energy (real part) distribution of the superradiant decay widths

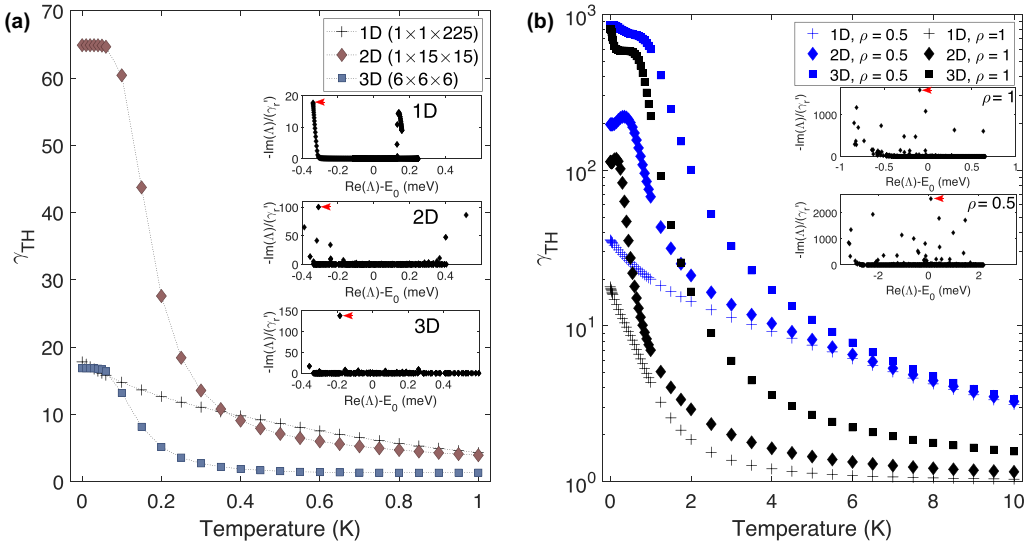

FIG. 5. Comparison of the robustness of superradiant enhancement to thermal decoherence in superlattices of (a) different dimensionalities ($a_x = a_y = 10$ nm, $N \simeq 225$) and (b) NC aspect ratios and dimensionalities ($a_x = a_y = 10$ nm, $N \simeq 1.06 \times 10^4$). Insets in panels (a) and (b) show the spectra of the Hamiltonian given in Eq. (1) for different dimensionalities and aspect ratios for the same N as in the corresponding figure. In the insets, superradiant eigenvalues are indicated by red arrows and we have defined $\gamma_r' \equiv \hbar\gamma_r/2$.

(imaginary part). The energy of a superlattice's most superradiant state strongly depends on its dimensionality.

In 1D and 2D, many superradiant states are concentrated near the edges of the eigenvalue spectrum [see insets in Fig. 5(a)]. In 3D, however, the most superradiant state lies at the center. Eigenvalue maps in the insets of Fig. 5(a) show that typical spectral widths are less than 1 meV. At very low temperatures ($\ll 10$ K $= 0.86$ meV$/k_B$), the system is in one of the lowest energy eigenstates with very high probability. At room temperature or higher ($T > 300$ K $= 25.8$ meV$/k_B$), the system is almost equally likely to be in any of the eigenstates. Thus, low-dimensional systems are favored at low temperature and small N due to the fact that there are more superradiant states close to the ground state, where the excitation concentrates.

Next, we consider the effect of ρ and N on robustness to thermal disorder. Figure 5(b) shows that superlattices of all dimensionalities with cuboidal ($\rho = 0.5$) NCs are more superradiant than those with cube-shaped ($\rho = 1$) NCs at all temperatures. This is because the lowest energy eigenvalues are more superradiant in such superlattices [Fig. 5(b), inset]. The spectral width in $\rho = 0.5$ NC superlattices is also over two times greater than that in $\rho = 1$ NC superlattices, further improving the superlattice's robustness to thermal disorder. Here, we have shown results for $N = 22^3 \simeq 1.06 \times 10^4$, because 3D superlattices are more superradiant than 1D and 2D in this regime. For much smaller N ($N < 1000$), 3D superlattices with cuboidal ($\rho = 0.5$) NCs are just as superradiant or slightly more superradiant than cubic NC superlattices at $T > 2$ K (see SM [47], Fig. S11).

However, for very low temperatures ($T \leqslant 2$ K) the opposite is true, because lowest energy eigenvalues, which contribute the most to radiative decay rate at low temperature, are *subradiant* in $\rho = 0.5$ NC superlattices when N is small. As we did for static disorder, we can further increase superradiance by combining the higher robustness to thermal disorder of the 2D superlattice geometry (which occurs when $N \lesssim 729$) and the higher/comparable robustness of cuboidal NC shape by arranging cuboidal NCs in a 2D superlattice [see SM [47], Fig. S7(b)].

The N dependence of SR's robustness to thermal disorder in 2D and 3D superlattices of cubic and cuboidal NCs is shown in SM [47] Fig. S12. γ_{TH} increases monotonically with N, reaching up to 10^2 at a temperature of about 6 K. The γ_{TH} for large N shown in Figs. 5 and S12 is only the lower bound due to cooperative robustness.

Our assumption that thermalization is the fastest timescale fails for large system sizes where photons could be emitted superradiantly before thermalization occurs. Based on prior calculations, in the presence of static disorder of the same order of magnitude as room-temperature energy, superradiant decay widths are ~16 meV. This corresponds to a superradiant lifetime of about 80 fs, which is much shorter than typical thermalization times of ~1 ps. Studying superradiance in this regime requires a nonequilibrium simulation of systems, which will be investigated in a future study.

IV. CONCLUSIONS AND OUTLOOK

We have analyzed the dependence of NC superlattice SR response with superlattice dimensionality, NC aspect ratio, and number of interacting dipoles. We show that a dimensional crossover occurs as the number of NCs increases in the superradiance enhancement from nanocrystal superlattices. Specifically, the main results obtained are the following:

(1) While one might think that 3D superlattices are always better for achieving large, robust SR responses, we show that this is not thee case for small numbers of interacting NCs. 2D superlattices made of less than 1000 NCs are more robust both to static and thermal disorder than 3D superlattices with the same number of NCs. Given that the coherent domains determining SR response in large NC superlattices can be quite small [8,16], our analysis can help guide future experiments.

(2) On the other hand, for large numbers of NCs, 3D superlattices always produce larger and more robust superradiance. Remarkably, we have shown that for large superlattices robustness to static disorder increases with superradiant decay width, which in 3D superlattices increases with the system size. This implies the emergence of cooperative robustness to disorder. Due to this effect we predict that large 3D superlattices can show superradiance even at room temperature, provided that the size fluctuations of the NCs composing the superlattice can be controlled. For example, if the average size is 10 nm, then the NC size variation should be less than 10%, that is, 10 nm $\pm$ 1 nm for the static disorder to be less than 25 meV.

(3) Changing NC aspect ratio can have a large impact on SR response. We show that decreasing aspect ratios by packing NCs more closely together results in stronger coupling and larger robustness of SR to both static and thermal disorder in all superlattice dimensionalities.

Several challenges remain. If the fluence of the incident radiation is high, the single-excitation assumption fails. Several NCs may be excited simultaneously, leading to a N^2 scaling of SR enhancement. In addition, when superradiant decay times are faster or comparable to the thermalization time, the decay rate of superlattices will deviate from the thermal average of the decay rates and the full nonequilibrium dynamics of the open quantum system must be taken into account.

ACKNOWLEDGMENTS

S.G., D.E., M.K., and B.J. thank the U.S. National Science Foundation (DMR-1952841) for financial support. We thank Fausto Borgonovi, Stefano Toso, Irina Gushchina, Zhuoming Zhang, Gabriele Rainò, Thilo Stöferle, and Maksym V. Kovalenko for helpful discussions. This research was supported in part by the Notre Dame Center for Research Computing through access to key computational resources.

[1] R. H. Dicke, Coherence in spontaneous radiation processes, Phys. Rev. **93**, 99 (1954).

[2] S. De Boer and D. A. Wiersma, Dephasing-induced damping of superradiant emission in j-aggregates, Chem. Phys. Lett. **165**, 45 (1990).

[3] H. Fidder, J. Knoester, and D. A. Wiersma, Superradiant emission and optical dephasing in j-aggregates, Chem. Phys. Lett. **171**, 529 (1990).

[4] M. O. Araújo, I. Krešić, R. Kaiser, and W. Guerin, Superradiance in a Large and Dilute Cloud of Cold Atoms in the Linear-Optics Regime, Phys. Rev. Lett. **117**, 073002 (2016).

[5] C. Bradac, M. T. Johnsson, M. van Breugel, B. Q. Baragiola, R. Martin, M. L. Juan, G. K. Brennen, and T. Volz, Room-temperature spontaneous superradiance from single diamond nanocrystals, Nat. Commun. **8**, 1205 (2017).

[6] T. Brandes, Coherent and collective quantum optical effects in mesoscopic systems, Phys. Rep. **408**, 315 (2005).

[7] M. Scheibner, T. Schmidt, L. Worschech, A. Forchel, G. Bacher, T. Passow, and D. Hommel, Superradiance of quantum dots, Nat. Phys. **3**, 106 (2007).

[8] G. Rainò, M. A. Becker, M. I. Bodnarchuk, R. F. Mahrt, M. V. Kovalenko, and T. Stöferle, Superfluorescence from lead halide perovskite quantum dot superlattices, Nature (London) **563**, 671 (2018).

[9] J. P. Philbin, J. Kelly, L. Peng, I. Coropceanu, A. Hazarika, D. V. Talapin, E. Rabani, X. Ma, and P. Narang, Room temperature single-photon superfluorescence from a single epitaxial cuboid nano-heterostructure, arXiv:2104.06452.

[10] I. Cherniukh, G. Rainò, T. Stöferle, M. Burian, A. Travesset, D. Naumenko, H. Amenitsch, R. Erni, R. F. Mahrt, M. I. Bodnarchuk *et al.*, Perovskite-type superlattices from lead halide perovskite nanocubes, Nature (London) **593**, 535 (2021).

[11] G. Findik, M. Biliroglu, D. Seyitliyev, J. Mendes, A. Barrette, H. Ardekani, L. Lei, Q. Dong, F. So, and K. Gundogdu, High-temperature superfluorescence in methyl ammonium lead iodide, Nat. Photonics **15**, 676 (2021).

[12] J. G. Bohnet, Z. Chen, J. M. Weiner, D. Meiser, M. J. Holland, and J. K. Thompson, A steady-state superradiant laser with less than one intracavity photon, Nature (London) **484**, 78 (2012).

[13] K. Higgins, S. Benjamin, T. Stace, G. Milburn, B. W. Lovett, and E. Gauger, Superabsorption of light via quantum engineering, Nat. Commun. **5**, 4705 (2014).

[14] F. Mattiotti, M. Sarovar, G. G. Giusteri, F. Borgonovi, and G. L. Celardo, Efficient light harvesting and photon sensing via engineered cooperative effects, New J. Phys. **24**, 013027 (2022).

[15] M. O. Scully and A. A. Svidzinsky, The super of superradiance, Science **325**, 1510 (2009).

[16] F. Mattiotti, M. Kuno, F. Borgonovi, B. Jankó, and G. L. Celardo, Thermal decoherence of superradiance in lead halide perovskite nanocrystal superlattices, Nano Lett. **20**, 7382 (2020).

[17] D. D. Blach, V. A. Lumsargis, D. E. Clark, C. Chuang, K. Wang, L. Dou, R. D. Schaller, J. Cao, C. W. Li, and L. Huang, Superradiance and exciton delocalization in perovskite quantum dot superlattices, Nano Lett. **22**, 7811 (2022).

[18] R. J. Bettles, S. A. Gardiner, and C. S. Adams, Cooperative ordering in lattices of interacting two-level dipoles, Phys. Rev. A **92**, 063822 (2015).

[19] R. Bettles, *Cooperative Interactions in Lattices of Atomic Dipoles* (Springer, New York, 2017).

[20] L. Bellando, A. Gero, E. Akkermans, and R. Kaiser, Cooperative effects and disorder: A scaling analysis of the spectrum of the effective atomic Hamiltonian, Phys. Rev. A **90**, 063822 (2014).

[21] E. Sierra, S. J. Masson, and A. Asenjo-Garcia, Dicke superradiance in ordered lattices: Dimensionality matters, Phys. Rev. Res. **4**, 023207 (2022).

[22] G. L. Celardo, G. G. Giusteri, and F. Borgonovi, Cooperative robustness to static disorder: Superradiance and localization in a nanoscale ring to model light-harvesting systems found in nature, Phys. Rev. B **90**, 075113 (2014).

[23] G. L. Celardo, P. Poli, L. Lussardi, and F. Borgonovi, Cooperative robustness to dephasing: Single-exciton superradiance in a nanoscale ring to model natural light-harvesting systems, Phys. Rev. B **90**, 085142 (2014).

[24] N. C. Chávez, F. Mattiotti, J. Méndez-Bermúdez, F. Borgonovi, and G. L. Celardo, Real and imaginary energy gaps: A

comparison between single excitation superradiance and superconductivity and robustness to disorder, Eur. Phys. J. B **92**, 1 (2019).

[25] T. Bienaimé, N. Piovella, and R. Kaiser, Controlled Dicke Subradiance from a Large Cloud of Two-Level Systems, Phys. Rev. Lett. **108**, 123602 (2012).

[26] T. Bienaimé, R. Bachelard, N. Piovella, and R. Kaiser, Cooperativity in light scattering by cold atoms, Fortschr. Phys. **61**, 377 (2013).

[27] M.-T. Rouabah, M. Samoylova, R. Bachelard, P. W. Courteille, R. Kaiser, and N. Piovella, Coherence effects in scattering order expansion of light by atomic clouds, J. Opt. Soc. Am. A **31**, 1031 (2014).

[28] S. J. Roof, K. J. Kemp, M. D. Havey, and I. M. Sokolov, Observation of Single-Photon Superradiance and the Cooperative Lamb Shift in an Extended Sample of Cold Atoms, Phys. Rev. Lett. **117**, 073003 (2016).

[29] P. Tighineanu, R. S. Daveau, T. B. Lehmann, H. E. Beere, D. A. Ritchie, P. Lodahl, and S. Stobbe, Single-Photon Superradiance from a Quantum Dot, Phys. Rev. Lett. **116**, 163604 (2016).

[30] M. C. Brennan, J. E. Herr, T. S. Nguyen-Beck, J. Zinna, S. Draguta, S. Rouvimov, J. Parkhill, and M. Kuno, Origin of the size-dependent Stokes shift in $CsPbBr_3$ perovskite nanocrystals, J. Am. Chem. Soc. **139**, 12201 (2017).

[31] S. Toso, D. Baranov, and L. Manna, Metamorphoses of cesium lead halide nanocrystals, Acc. Chem. Res. **54**, 498 (2021).

[32] X. Sui, X. Gao, X. Wu, C. Li, X. Yang, W. Du, Z. Ding, S. Jin, K. Wu, T. C. Sum *et al.*, Zone-folded longitudinal acoustic phonons driving self-trapped state emission in colloidal CdSe nanoplatelet superlattices, Nano Lett. **21**, 4137 (2021).

[33] M. A. Becker, R. Vaxenburg, G. Nedelcu, P. C. Sercel, A. Shabaev, M. J. Mehl, J. G. Michopoulos, S. G. Lambrakos, N. Bernstein, J. L. Lyons *et al.*, Bright triplet excitons in caesium lead halide perovskites, Nature (London) **553**, 189 (2018).

[34] D. Baranov, S. Toso, M. Imran, and L. Manna, Investigation into the photoluminescence red shift in cesium lead bromide nanocrystal superlattices, J. Phys. Chem. Lett. **10**, 655 (2019).

[35] D. Baranov, A. Fieramosca, R. X. Yang, L. Polimeno, G. Lerario, S. Toso, C. Giansante, M. D. Giorgi, L. Z. Tan, D. Sanvitto *et al.*, Aging of self-assembled lead halide perovskite nanocrystal superlattices: Effects on photoluminescence and energy transfer, ACS Nano **15**, 650 (2021).

[36] M. O'Neill, *The Merck Index, An Encyclopedia of Chemicals, Drugs and Biologicals* (Merck Research Laboratories, Whitehouse Station, NJ, 2006).

[37] S. Horikoshi, H. Abe, T. Sumi, K. Torigoe, H. Sakai, N. Serpone, and M. Abe, Microwave frequency effect in the formation of au nanocolloids in polar and non-polar solvents, Nanoscale **3**, 1697 (2011).

[38] J. L. Movilla, J. Planelles, and J. I. Climente, Dielectric confinement enables molecular coupling in stacked colloidal nanoplatelets, J. Phys. Chem. Lett. **11**, 3294 (2020).

[39] X. Peng, L. Manna, W. Yang, J. Wickham, E. Scher, A. Kadavanich, and A. P. Alivisatos, Shape control of CdSe nanocrystals, Nature (London) **404**, 59 (2000).

[40] S. Ithurria and B. Dubertret, Quasi 2D colloidal CdSe platelets with thicknesses controlled at the atomic level, J. Am. Chem. Soc. **130**, 16504 (2008).

[41] S. Ithurria, G. Bousquet, and B. Dubertret, Continuous transition from 3D to 1D confinement observed during the formation of CdSe nanoplatelets, J. Am. Chem. Soc. **133**, 3070 (2011).

[42] H. Yu, J. Li, R. A. Loomis, P. C. Gibbons, L.-W. Wang, and W. E. Buhro, Cadmium selenide quantum wires and the transition from 3D to 2D confinement, J. Am. Chem. Soc. **125**, 16168 (2003).

[43] Y.-H. Liu, V. L. Wayman, P. C. Gibbons, R. A. Loomis, and W. E. Buhro, Origin of high photoluminescence efficiencies in CdSe quantum belts, Nano Lett. **10**, 352 (2010).

[44] J. W. Grebinski, K. L. Hull, J. Zhang, T. H. Kosel, and M. Kuno, Solution-based straight and branched CdSe nanowires, Chem. Mater. **16**, 5260 (2004).

[45] J. Shamsi, A. S. Urban, M. Imran, L. De Trizio, and L. Manna, Metal halide perovskite nanocrystals: Synthesis, post-synthesis modifications, and their optical properties, Chem. Rev. **119**, 3296 (2019).

[46] J. Shamsi, P. Rastogi, V. Caligiuri, A. L. Abdelhady, D. Spirito, L. Manna, and R. Krahne, Bright-emitting perovskite films by large-scale synthesis and photoinduced solid-state transformation of $CsPbBr_3$ nanoplatelets, ACS Nano **11**, 10206 (2017).

[47] See Supplemental Material at http://link.aps.org/supplemental/10.1103/PhysRevResearch.5.023068 for Figs. S1–S12.

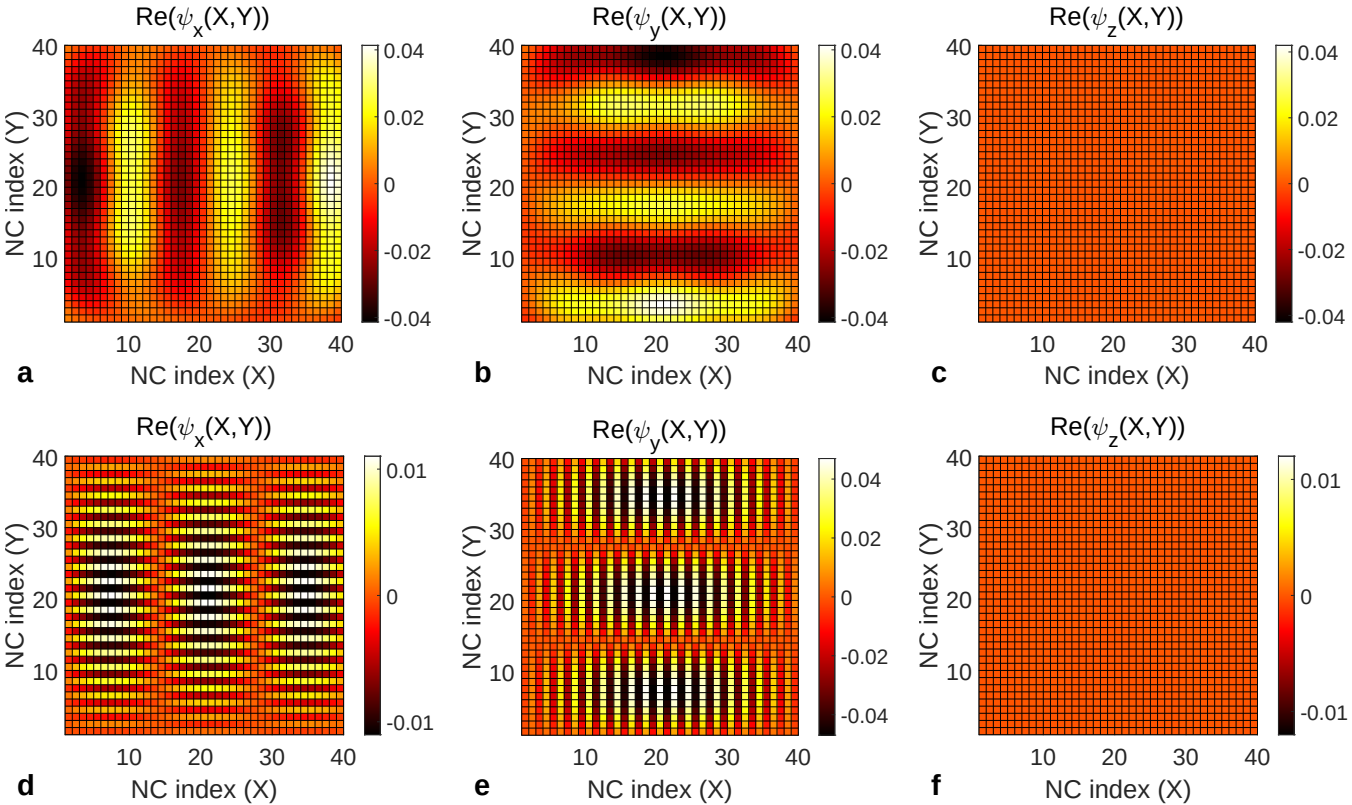

FIG. S1. (Supplementary Information) Real part of the superradiant eigenvector (a-c) with $\gamma_{\rm enh} = 58.9$ and a typical ommstrongly subradiant eigenvector (d-f) with $\gamma_{\rm enh} = 8.4 \times 10^{-5}$, of a 40×40 2D superlattice with $a_x = a_y = 20$ nm. $\psi_j(X, Y)$ is the component of the wavefunction for the dipole in the j-direction in the nanocrystal at position (X, Y).

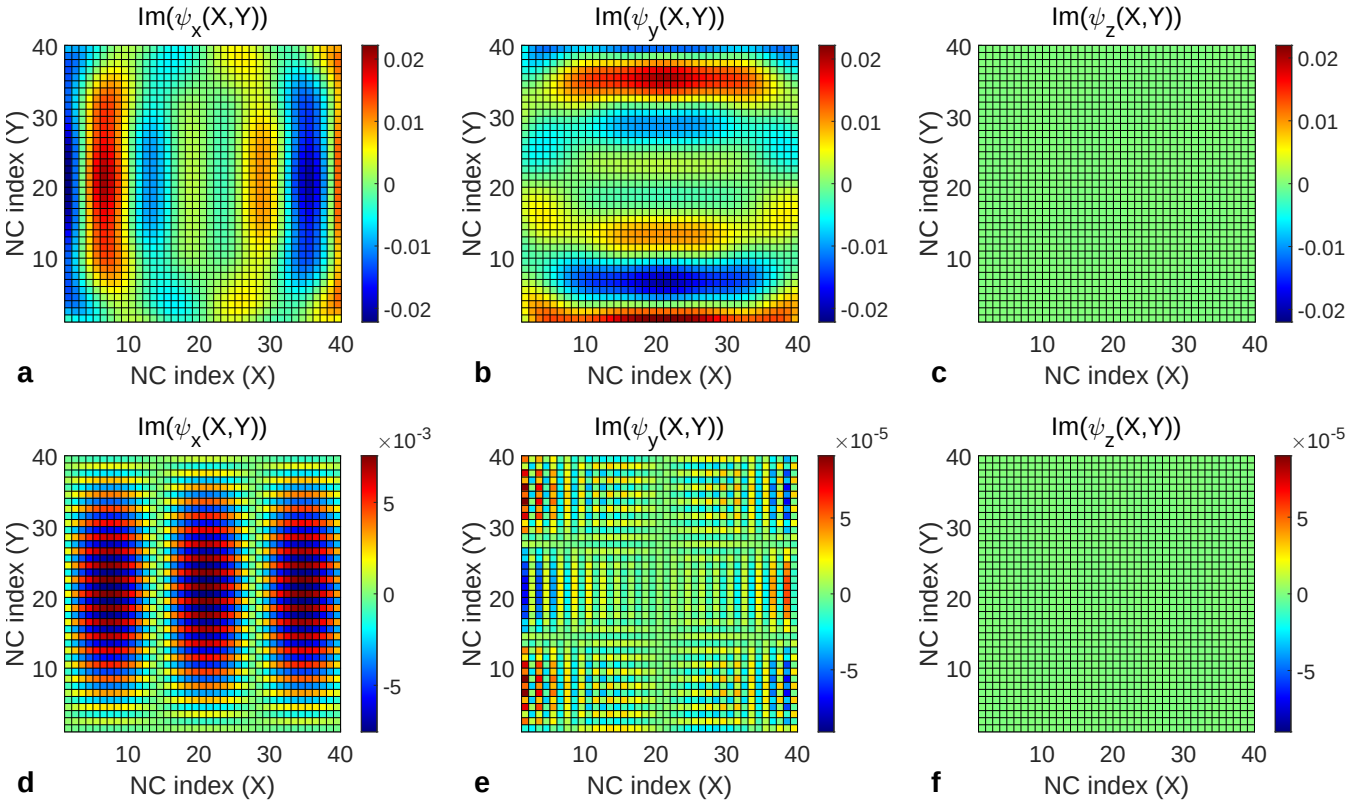

FIG. S2. (Supplementary Information) Imaginary part of the superradiant eigenvector (a-c) with $\gamma_{\rm enh} = 58.9$ and a typical strongly subradiant eigenvector (d-f) with $\gamma_{\rm enh} = 8.4 \times 10^{-5}$, of a 40×40 2D superlattice with $a_x = a_y = 20$ nm. $\psi_j(X, Y)$ is the component of the wavefunction for the dipole in the j-direction in the nanocrystal at position (X, Y).

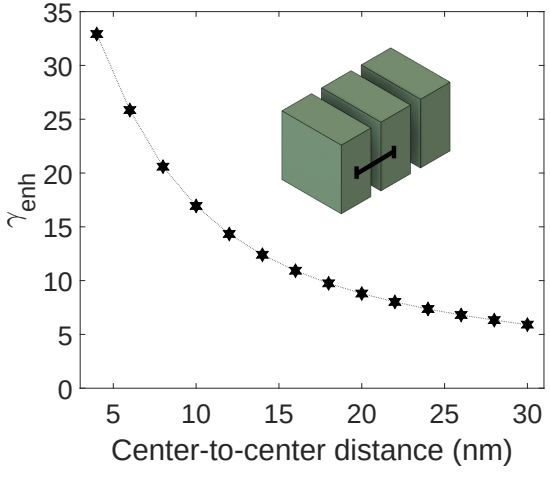

FIG. S3. (Supplementary Information) Dependence of superradiant enhancement on the center-to-center distance for 1D superlattices ($N = 50$). The edge-lengths of the NCs normal to the superlattice do not affect γ_{enh} as long as we remain in the weak confinement regime.

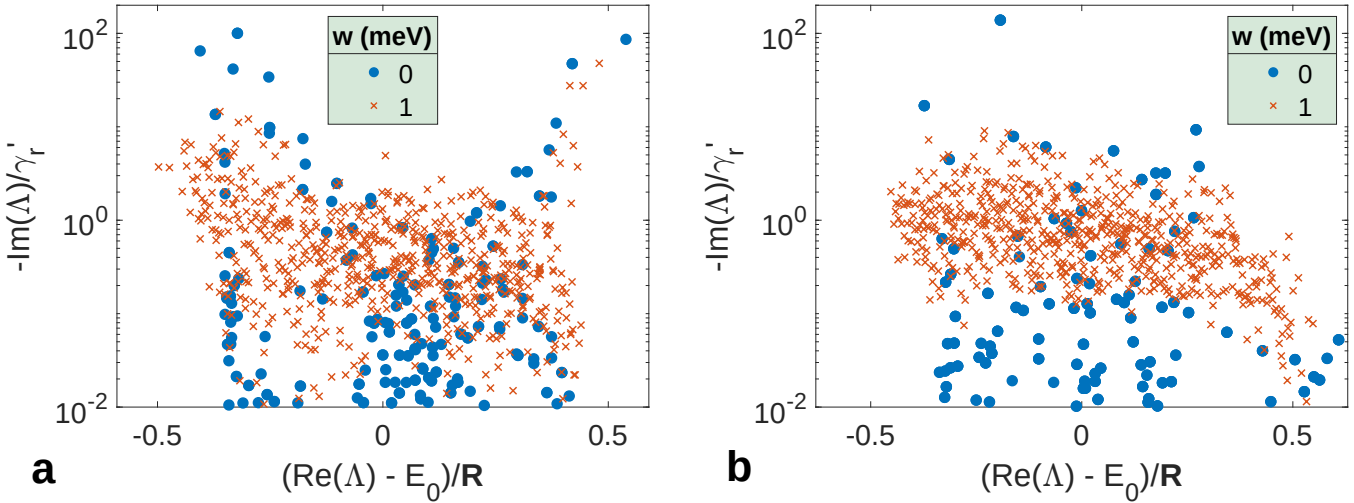

FIG. S4. (Supplementary Information) Spectra of (a) 2D ($N = 225$) and (b) 3D ($N = 216$) superlattices ($a_x = a_y = a_z = 10$ nm) of cubic nanocrystals in the absence (blue circles) and 1 meV (red crosses) of static disorder normalized by the range of real values (**R**).

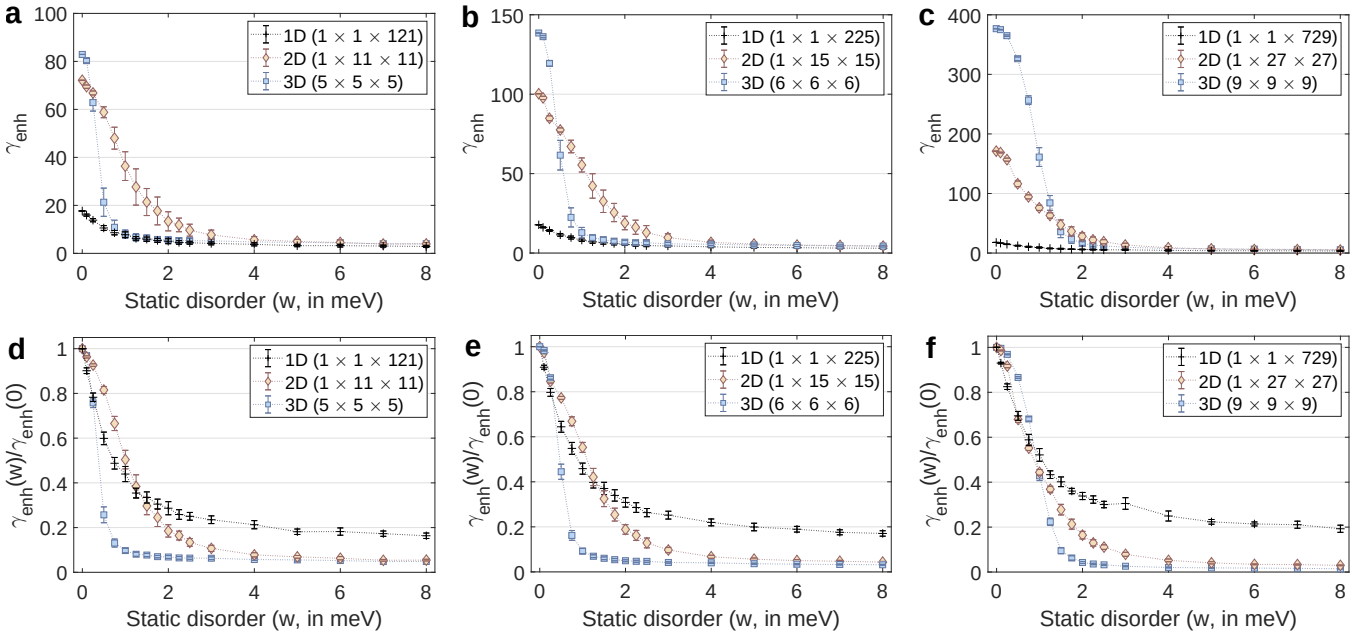

FIG. S5. (Supplementary Information) Comparison of the robustness of the superradiant enhancement factor (γ_{enh}) to static disorder in superlattices ($a_x = a_y = a_z = 10$ nm) of different dimensionalities. (a,d) $N \simeq 121$, (b,e) $N \simeq 225$ and (c,f) $N = 729$. The top row (a-c) shows the absolute enhancement factor, while the bottom row (d-f) shows the relative enhancement.

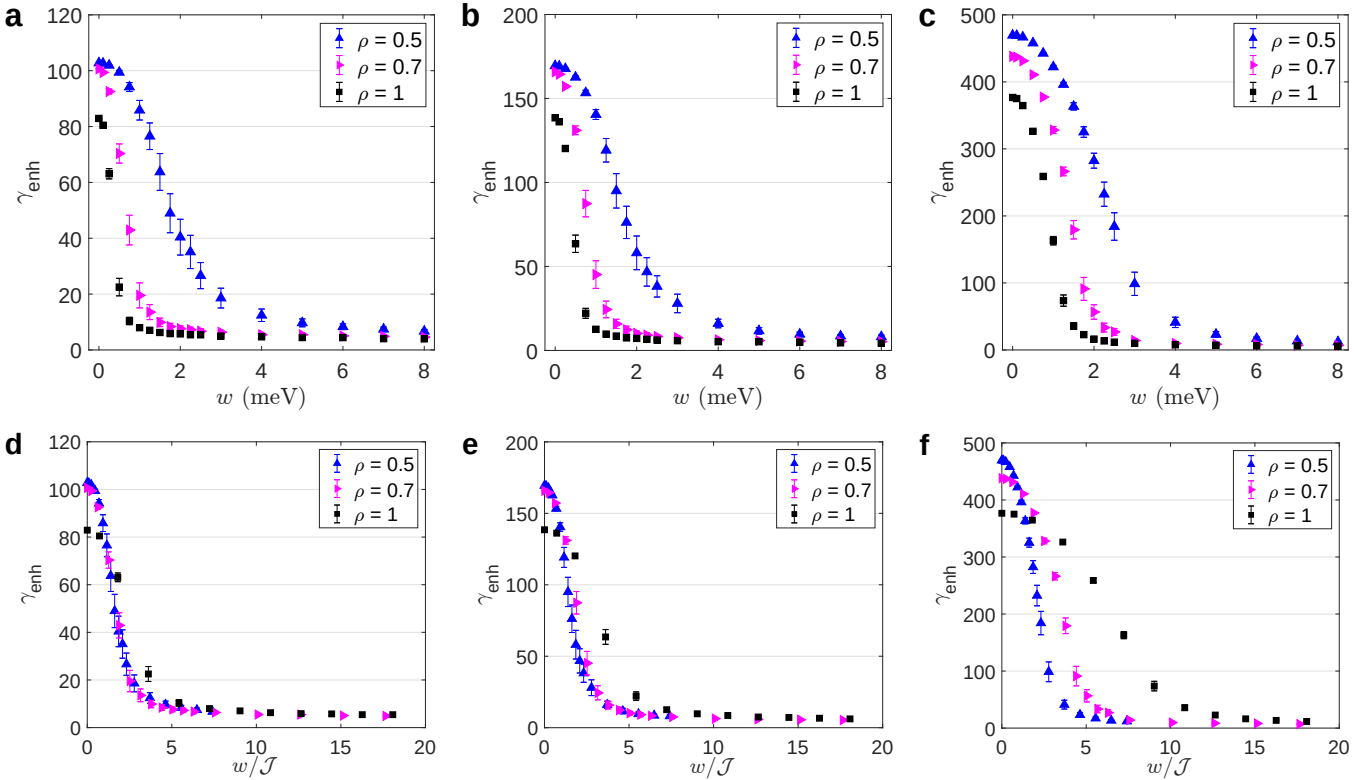

FIG. S6. (Supplementary Information) Comparison of the robustness of the superradiant enhancement factor ($\gamma_{\rm enh}$) to static disorder (a-c) and the ratio of static disorder to the nearest neighbor coupling (d-f) in superlattices ($a_x = a_y = a_z = 10$ nm) with different NC aspect ratios. (a, d) $N \simeq 125$ ($5 \times 5 \times 5$), (b, e) $N = 216$ ($6 \times 6 \times 6$) and (c, f) $N = 729$ ($9 \times 9 \times 9$).

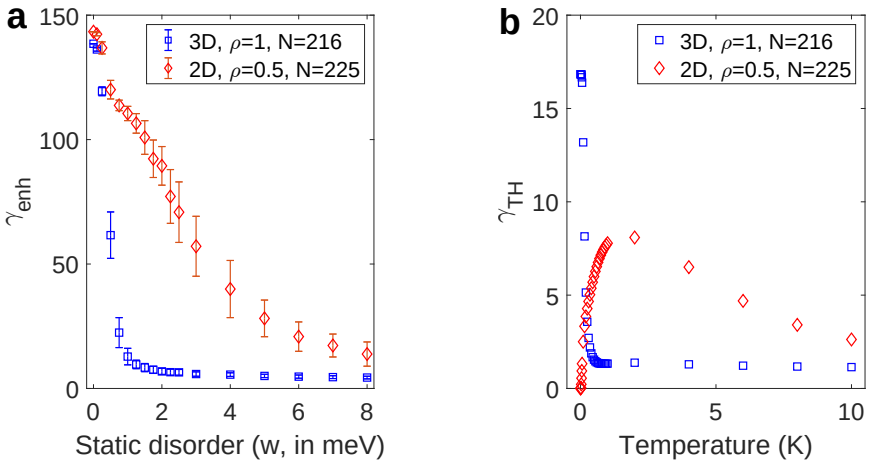

FIG. S7. (Supplementary Information) Comparison of the robustness to (a) static and (b) thermal disorder of cuboidal ($\rho = 0.5$) NCs in a 2D superlattice with cubic NCs in a 3D superlattice ($N = 216/225$, $a_x = a_y = 10$ nm).

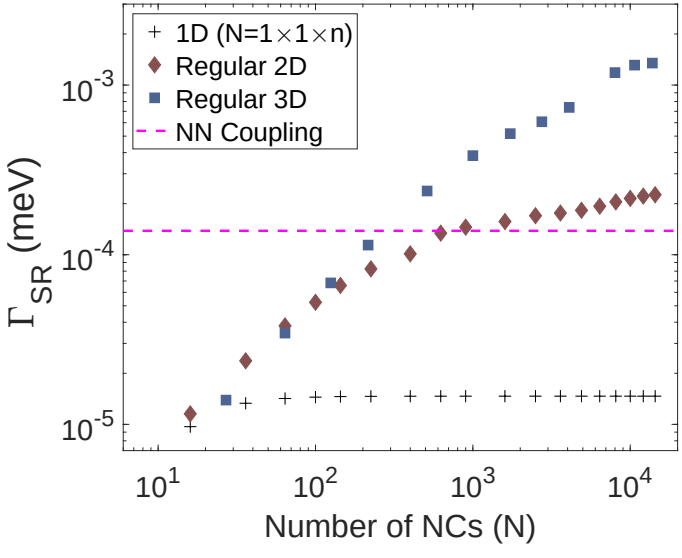

FIG. S8. (Supplementary Information) Comparison of the maximum possible SR enhancement (in meV) from different superlattice dimensionalities composed of cube-shaped NCs with a center-to-center distance of 10 nm (i.e. $a_x = a_y = a_z =$ 10 nm). The pink line shows the nearest neighbor coupling ($\mathcal{J}$) between NCs.

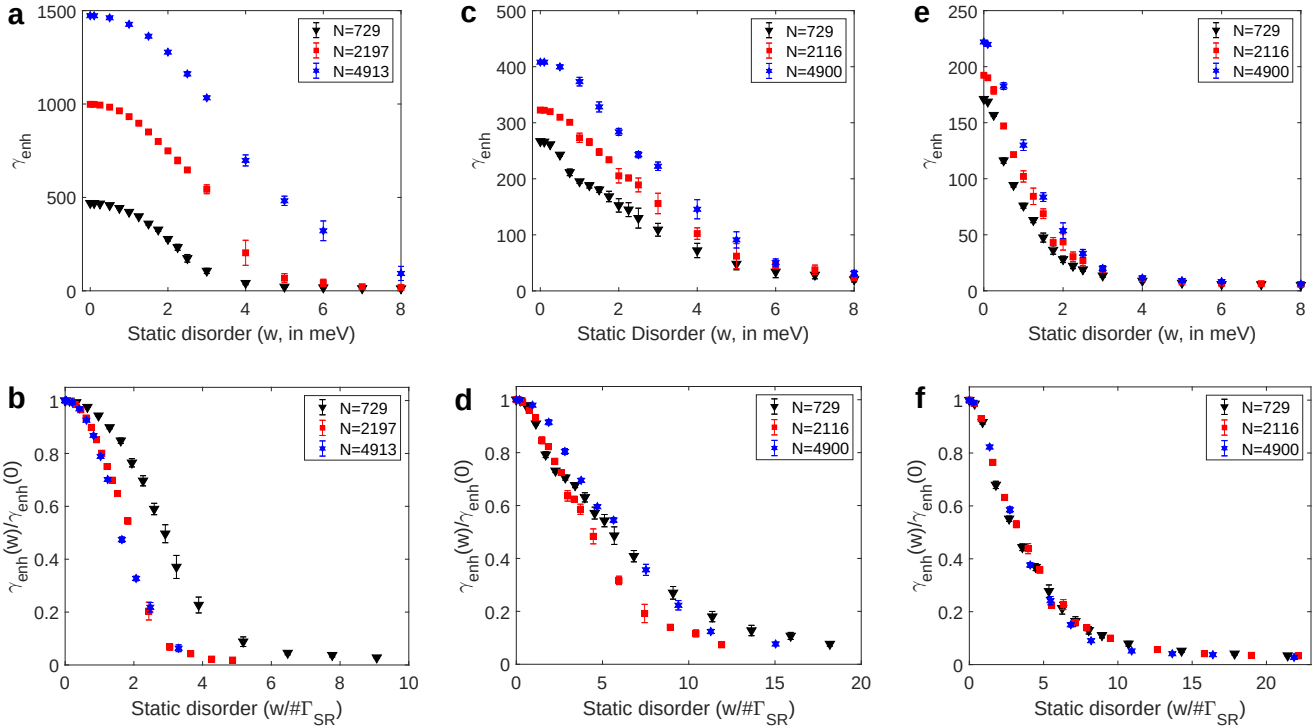

FIG. S9. (Supplementary Information) Robustness of 3D (a, b) and 2D (c, d, e, f) superlattices of cuboidal (a, b, c, d) ($\rho = 0.5$) and cubic (e, f) NCs to static disorder for different N ($a_x = a_y = 10$ nm). The top row (a, c, e) shows the absolute enhancement factors while the bottom row (b, d, f) shows relative enhancement factors.

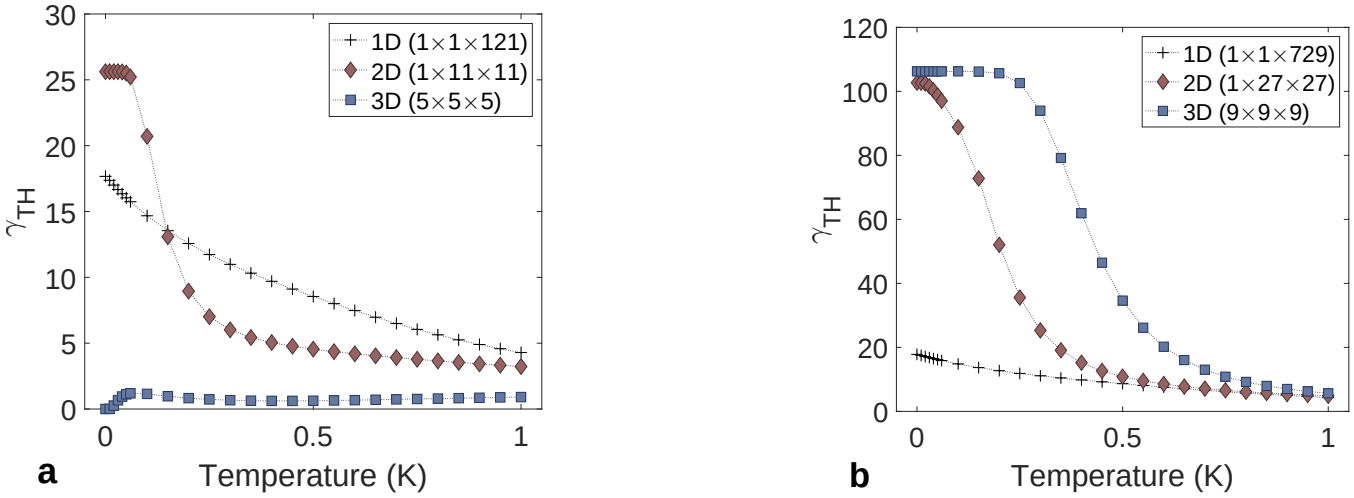

FIG. S10. (Supplementary Information) Comparison of the robustness of the superradiant enhancement factor (γ_{TH}) to thermal disorder in superlattices ($a_x = a_y = a_z = 10$ nm) of different dimensionalities. (a) $N \simeq 125$ and (b) $N = 729$.

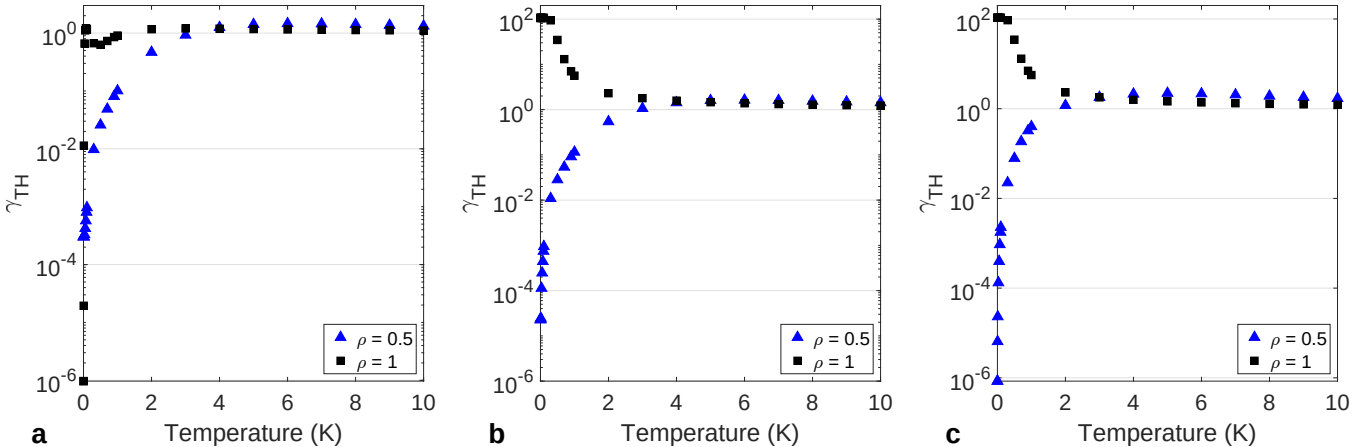

FIG. S11. (Supplementary Information) Comparison of the robustness of the superradiant enhancement factor (γ_{TH}) to thermal disorder in superlattices ($a_x = a_y = 10$ nm) with different NC aspect ratios. (a) $N = 125$, (b) $N = 225$ and (c) $N = 729$.

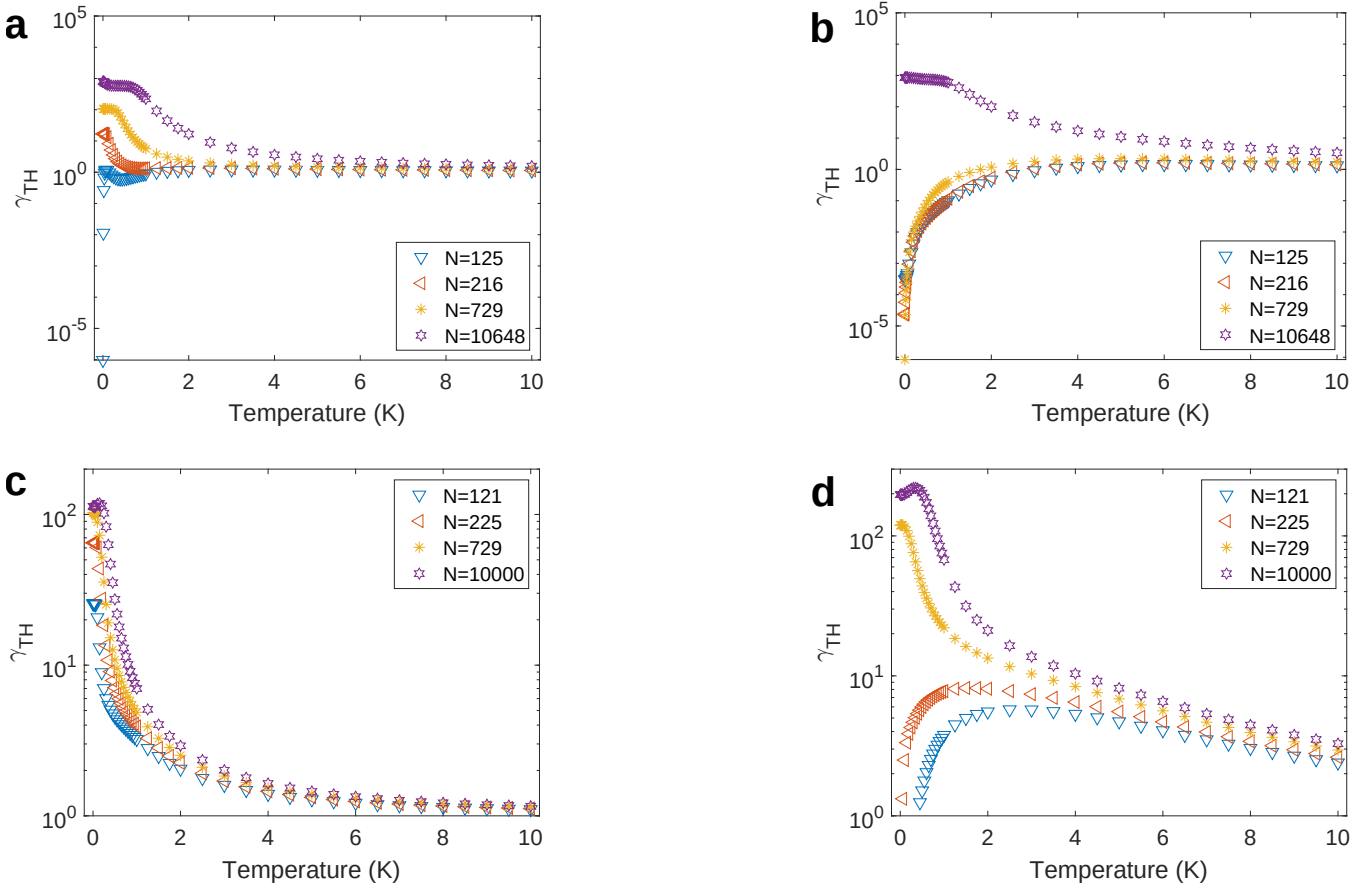

FIG. S12. (Supplementary Information) Robustness of 3D (a, b) and 2D (c, d) superlattices of cubic ($\rho = 1$, (a, c)) and cuboidal NCs ($\rho = 0.5$, (b, d)) to thermal disorder for different N ($a_x = a_y = 10$ nm).